



Article

Unifying thermodynamic and mechanical stability in perovskites: a computational approach for advanced applications

Coskun Firat*

Istanbul Technical University, Energy Institute, Istanbul, Türkiye

ARTICLE INFO

Article history:

Received 25 March 2025

Received in revised form

07 May 2025

Accepted 15 May 2025

Keywords:

Perovskite stability, Thermodynamic-mechanical integration, combined stability index, Computational analysis, Material design for durability

*Corresponding author

Email address:

coskun.firat@itu.edu.tr

DOI: 10.55670/fpll.fusus.3.3.4

ABSTRACT

Perovskite materials hold immense potential for advanced technologies, yet their practical deployment is hindered by an insufficient understanding of the interplay between thermodynamic and mechanical stability. This study bridges this critical gap by developing a unified computational framework that integrates both stability dimensions, enabling the rational design of perovskites for demanding applications. Leveraging pre-computed density functional theory data from The Materials Project and AFLOW databases, 44 perovskite materials are analyzed. Thermodynamic stability is assessed via formation energy and energy above hull, while mechanical stability is quantified through bulk modulus, shear modulus, and Pugh's ratio. A novel combined stability index is introduced, employing geometric mean aggregation of normalized metrics to prioritize balanced performance. Key findings reveal that Ba-based perovskites exhibit superior thermodynamic stability and mechanical resilience. This work provides a computational blueprint for synthesizing perovskites tailored to applications requiring durability under thermal and mechanical stress, such as photovoltaics and catalysis. By correlating composition-structure-property relationships, the study advances the design of next-generation materials, emphasizing the necessity of holistic stability metrics.

1. Introduction

Perovskite materials, with their general formula ABX_3 , have emerged as a cornerstone of modern materials science due to their exceptional optoelectronic, catalytic, and mechanical properties [1]. These materials underpin advancements in solar cells, light-emitting diodes, solid oxide fuel cells, and piezoelectric devices, among others. However, their practical implementation is often hindered by challenges related to stability under operational conditions. Thermodynamic stability [2-4] in perovskites has been widely studied using metrics such as formation energy and energy above the hull. For instance, Ba-based perovskites are renowned for their superior thermodynamic stability [5-7], whereas materials with high energy above hull values are prone to decomposition [8]. However, these studies have focused mainly on isolated thermodynamic properties [9-11], neglecting how mechanical stability [12-14] influences overall performance. Conversely, mechanical stability metrics like bulk modulus [15], shear modulus [16], and Pugh's ratio

(B/G) [12,17] have been used to classify perovskites as brittle or ductile [18-20], with K-based perovskites [21] demonstrating excellent mechanical properties. Yet, the interplay between thermodynamic and mechanical stability remains poorly understood, limiting the rational design of perovskites that can withstand real-world stresses such as thermal cycling or mechanical loading [22-23]. Previous studies have made significant strides in exploring thermodynamic or mechanical stability in isolation, but few have considered these aspects together in a cohesive framework [24-27]. This disconnect is problematic for applications where both forms of stability are critical. For example, a material with excellent thermodynamic stability but poor mechanical properties may fail under stress, while a mechanically robust material with poor thermodynamic stability may decompose during operation [28]. Bridging this gap requires a holistic approach that integrates thermodynamic and mechanical stability metrics, enabling the design of perovskites with balanced properties. In this

study, three key questions are addressed: How can thermodynamic and mechanical stability be unified into a single framework for perovskites? What composition-structure-property relationships govern their combined stability? And which materials exhibit optimal stability profiles for advanced applications? To answer these questions, pre-computed DFT data from both The Materials Project and AFLOW for 44 perovskites with different crystal systems are analyzed [29,30]. Thermodynamic parameters (formation energy, energy above hull) and mechanical properties (bulk modulus, shear modulus) are evaluated using Python-based computational tools. A combined stability index is introduced to unify these metrics, enabling systematic identification of materials with optimal stability profiles. This work makes several key contributions. First, a unified stability framework is established, which integrates thermodynamic and mechanical metrics, providing a holistic view of perovskite stability. Second, the composition-structure-property relationships are revealed, showing that Ba-based perovskites excel in thermodynamic and mechanical stability. Notably, tantalum-containing compounds consistently outperform their niobium counterparts in combined stability metrics. Third, promising candidates such as KTaO_3 (high mechanical strength), $\text{Ba}_2\text{TaInO}_6$ (exceptional thermodynamic stability), and $\text{Ba}_2\text{TaInO}_6$, BaNbO_3 (balanced stability) are identified. These findings offer a computational blueprint for designing next-generation perovskites, with implications for energy conversion, catalysis, and electronics. The practical relevance of this work lies in its ability to guide the synthesis of stable perovskites for applications requiring both durability and performance. For instance, thermodynamically and mechanically robust perovskites could enhance the longevity of solar cells, improve catalytic efficiency in harsh environments, or develop reliable high-temperature sensors.

2. Methodology

This study analyzes a dataset of 44 perovskite materials with ABX_3 and related stoichiometries, leveraging pre-computed density functional theory (DFT) [31] data from The Materials Project and AFLOW databases. The dataset comprises materials with cubic, pseudo-cubic, tetragonal or trigonal symmetry [32], spanning diverse compositions of A-site cations (Ba, Sr, Ca, K, Na) [33,34] and B-site cations (Ti, Zr, Nb, Ta) [35,36], enabling systematic exploration of composition-stability relationships. The DFT calculations were performed using the Vienna Ab initio Simulation Package (VASP) [37] with the Perdew-Burke-Ernzerhof (PBE) exchange-correlation functional [38], ensuring consistency with widely accepted computational standards. The dataset includes the following key parameters:

- Material identification: Chemical formula, standardized formula notation, and unique material ID.
- Crystal structure: Space group, lattice parameters, and atomic positions.
- Electronic properties: Bandgap and electronic structure classification (metal, semiconductor, or insulator).
- Thermodynamic stability: Formation energy per atom, energy above hull (relative to the convex hull), and stability classification.
- Mechanical properties: Voigt-Reuss-Hill (VRH) averaged bulk modulus, shear modulus, and elastic constants where available.

Python-based computational tools (pandas, NumPy, matplotlib, seaborn) were employed to process and analyze

the dataset [39]. Derived mechanical properties, including Pugh's ratio (B/G), Poisson's ratio, and Vickers hardness, were calculated using empirical relationships. A combined stability index was developed to unify thermodynamic and mechanical stability metrics, enabling quantitative comparison of materials. Statistical methods, including correlation analysis and classification algorithms, were applied to identify trends in composition-structure-property relationships. To ensure reproducibility, all computational workflows- from data retrieval to visualization- were structured using open-source libraries, with custom functions validated against reference calculations. The methodology emphasizes transparency in parameter derivation and error handling, particularly for entries with anomalous mechanical properties (e.g., negative shear moduli).

2.1 Thermodynamic and mechanical stability analysis

Thermodynamic stability was evaluated using two key metrics: the formation energy per atom (E_f) and the energy above hull (E_{hull}). The formation energy, defined as [30]:

$$E_f = \frac{E_{\text{compound}} - \sum_i n_i E_i}{N} \quad (1)$$

Eq (1) quantifies the energy released or required to form a compound from its constituent elements. Here, E_{compound} is the total energy of the perovskite, n_i and E_i represent the number of atoms and reference energy of element i in its standard state, and N is the total number of atoms in the compound. The energy above the hull (E_{hull}), calculated as [30]:

$$E_{hull} = E_{\text{compound}} - E_{\text{convex hull}} \quad (2)$$

Eq (2) measures the energy difference between a compound and the most stable phase(s) at its composition, where $E_{\text{convex hull}}$ corresponds to the lowest-energy configuration of stable phases.

Materials were categorized into stability classes based on E_{hull} values:

- Stable: $E_{hull} = 0$
- Very likely stable: $0 < E_{hull} < 0.025$ eV/atom
- Likely stable: $0.025 \leq E_{hull} < 0.05$ eV/atom
- Potentially metastable: $0.05 \leq E_{hull} < 0.1$ eV/atom
- Likely unstable: $E_{hull} \geq 0.1$ eV/atom.

Statistical analyses, including mean, standard deviation, and extreme values, were applied to characterize the distribution of thermodynamic parameters. Correlation studies further identified relationships between composition and stability metrics.

Mechanical stability is assessed using bulk modulus (B), shear modulus (G), and derived parameters. The Voigt-Reuss-Hill (VRH) averaging scheme has been employed to compute isotropic values of B and G from the anisotropic elastic tensor for data in the databases. Pugh's ratio (B/G) classifies materials as ductile ($B/G > 1.75$) or brittle ($B/G < 1.75$). Derived mechanical properties included: Young's modulus [40,41]:

$$E = \frac{9BG}{3B+G} = 2G(1 + \nu) \quad (3)$$

Poisson's ratio [40,41]:

$$\nu = \frac{3B-2G}{2(3B+G)} \quad (4)$$

Vickers hardness [42]:

$$H_v \approx 0.92 \left(\frac{G}{B}\right)^{1.137} G^{0.708} \quad (5)$$

Simplified elastic anisotropy index (derived from the universal anisotropy index [43]):

$$A^{approx} = \frac{5G}{B} + \frac{B}{5G} - \frac{6}{5} \quad (6)$$

Statistical distributions of mechanical properties were analyzed, and correlation matrices were constructed to explore relationships between composition and mechanical behavior.

2.2 Combined stability assessment

To holistically evaluate both thermodynamic and mechanical stability, a combined stability index integrating normalized values of E_{hull} , B , G , and Pugh's ratio is developed. This index enables systematic ranking of materials based on their ability to balance competing stability requirements, critical for applications demanding both long-term phase persistence and mechanical resilience. The assessment framework follows four key steps:

Normalization: Each parameter (E_{hull} , B , G , B/G) was scaled to a 0–1 range using min-max normalization to eliminate unit dependency and ensure equal weighting. For a parameter X , the normalized value X_{norm} is calculated as:

$$X_{norm} = \frac{X - X_{min}}{X_{max} - X_{min}} \quad (7)$$

where X_{min} and X_{max} represent the minimum and maximum values of X across the dataset. For E_{hull} , lower values indicate greater stability, so the normalization was inverted ($1 - X_{norm}$).

Weighting: Parameters were assigned weights reflecting their relevance to specific applications. For general-purpose evaluation, equal weights ($\omega_i = 0.25$) were applied to all parameters, ensuring unbiased prioritization of thermodynamic and mechanical stability.

Aggregation: The weighted parameters were combined using the geometric mean to compute the stability index (S_{index}) for each material [44]:

$$S_{index} = \left(\prod_{i=1}^n X_{i,norm}^{\omega_i}\right)^{1/\sum \omega_i} \quad (8)$$

Unlike arithmetic averaging, the geometric mean penalizes materials with extreme weaknesses in any stability dimension, favoring balanced performance.

Classification: Materials were categorized into four stability classes: For classification, thresholds were defined for each property (E_{hull} , E_f , B , G , and Pugh's ratio). These thresholds are used to classify materials into different stability categories. A categorization function was defined to evaluate each material based on the defined thresholds. The function first categorizes the material based on E_{hull} . Then, it adjusts the stability category based on mechanical properties (B , G , and Pugh's ratio). Finally, it considers E_f to provide a holistic assessment. The combined stability category will be like: Stable (Strong Mechanical Properties) (Low Formation Energy), Very Likely Stable (Moderate Mechanical Properties) (Moderate Formation Energy), Likely Stable (Brittle) (Low Formation Energy), Potentially Metastable (Brittle) (Low Formation Energy), Likely Unstable (Weak Mechanical Properties) (High Formation Energy), Unknown (for materials with missing data).

3. Computational details and the results

The dataset for this study originated from the Materials Project and AFLOW databases, from which 1070 cubic perovskite materials with ABX_3 and related stoichiometries were initially extracted. However, only 44 of these materials contained complete mechanical property data (bulk modulus, shear modulus, etc.), necessitating a focused analysis on this subset to unify thermodynamic and mechanical stability metrics. All computational workflows, including data processing, statistical analysis, and visualization, were implemented in Python 3.8 using the following libraries:

- Pandas and NumPy for data manipulation and numerical computations.
- Matplotlib and seaborn for generating visualizations.
- Custom functions for specialized calculations, such as the combined stability index and normalized parameter aggregation.

Key visualization techniques were employed to elucidate structure-property relationships:

- a. Scatter plots to examine correlations between thermodynamic and mechanical parameters.
- b. Heatmaps to visualize multivariate relationships across stability metrics.
- c. Bar charts to compare key properties (e.g., formation energy, bulk modulus) across materials.
- d. Radar plots for multi-parameter comparison of top-performing candidates.

The computational workflow was designed for reproducibility:

- Data processing steps were systematically documented, including handling of missing values and normalization procedures.
- Validation against reference calculations (e.g., cross-checking DFT-derived properties with literature values) ensured robustness.
- The final dataset of 44 materials, along with analysis scripts, is archived to facilitate reproducibility.

This approach enabled the integration of thermodynamic stability (formation energy, energy above hull) and mechanical stability (bulk modulus, shear modulus, Pugh's ratio) into a unified framework. By focusing on materials with complete datasets, the combined stability index could be rigorously applied to identify candidates with balanced performance for advanced applications. The results for the first five stable materials are given in Table 1.

In Figure 1, the thermodynamic stability distribution of 44 perovskite materials based on their E_{hull} values are illustrated.

The distribution shows a sharp decline in frequency as E_{hull} increases, indicating that most materials are stable or very likely stable, with fewer materials being metastable or unstable. The dashed lines provide clear visual thresholds for the stability categories, aiding in the quick assessment of material stability. Figure 2 indicates the Pugh's ratio distribution of 44 materials. It can be seen that most materials have a Pugh's ratio clustered around 2, indicating a tendency towards ductility. The red dashed line at 1.75 clearly marks the boundary between ductile and brittle materials, making it easy to identify the classification of each material. The distribution shows a sharp peak around the ductile region, with a rapid decline in frequency as the ratio increases, indicating that most materials are ductile. A few materials have significantly higher Pugh's ratios, suggesting they are exceptionally ductile.

Table 1. Thermodynamic, mechanical properties, and combined index for some stable materials

Code	Formula	Crystal system	E_{hull} (eV/atom)	E_f (eV/atom)	B (Gpa)	G (Gpa)	Pugh's ratio	Combined index
M7	Ca ₂ Ta ₂ O ₇	Cubic	0.000789	-3.4826	148.2	97.79	1.5155	78
M13	BaTiO ₃	Cubic	0.014788	-3.4775	160	106.6	1.5009	74
M18	KTaO ₃	Cubic	0	-3.0716	184.6	121.3	1.5218	44.5
M19	BaZrO ₃	Cubic	7.17E-05	-3.6392	147.6	91.03	1.6214	78
M28	SrFeO ₃	Cubic	0	-2.223	128.6	80.35	1.6004	99.5

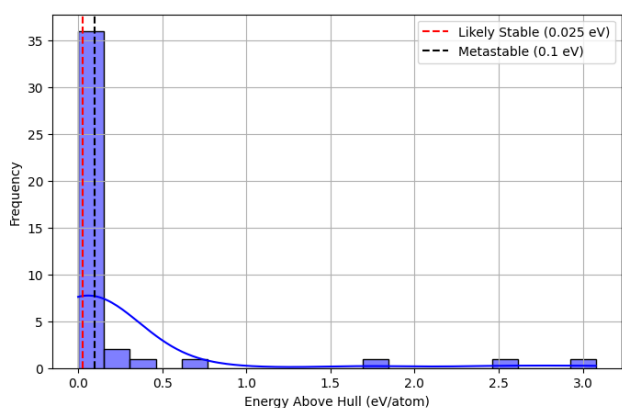


Figure 1. Thermodynamic stability distribution of perovskites based on E_{hull}

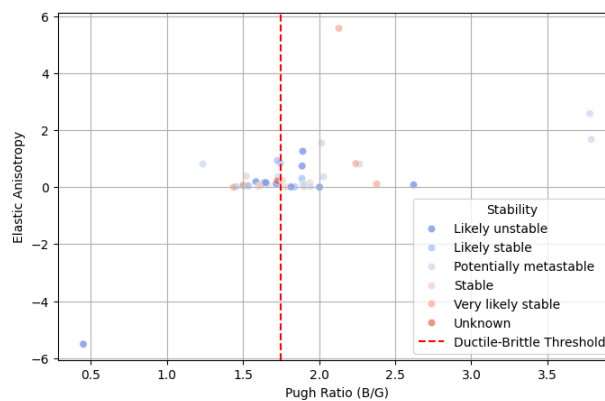


Figure 3. Relationship between Pugh's ratio (B/G) and elastic anisotropy for various materials

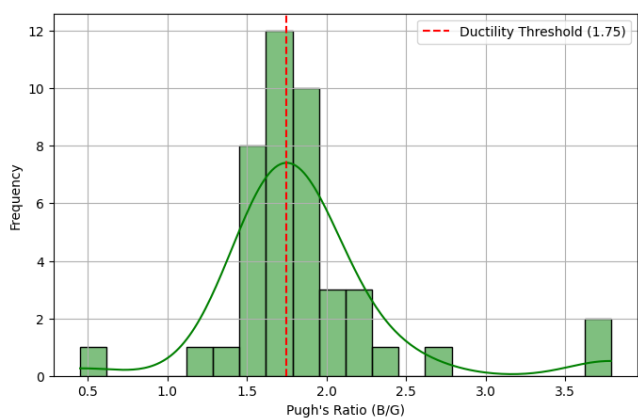


Figure 2. Distribution of Pugh's ratio of the perovskite materials

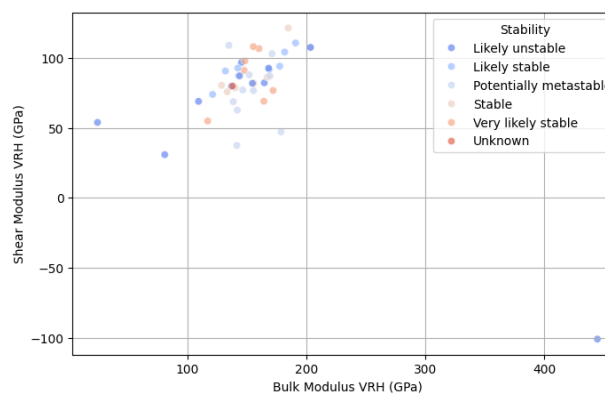


Figure 4. The relationship between the bulk modulus and shear modulus for various materials

Figure 3 illustrates the relationship between Pugh's ratio (B/G) and elastic anisotropy for various materials. In Figure 3, the red dashed line at B/G = 1.75 separates ductile materials (right) from brittle ones (left). Most stable materials have low anisotropy and are near the ductile-brittle threshold. A few outliers show significant anisotropy or extreme Pugh's ratios. Figure 4 shows the relationship between the bulk modulus (B) and shear modulus (G) for various materials.

Most materials are clustered between 100-200 GPa for bulk modulus and 50-150 GPa for shear modulus. A few outliers have significantly higher or lower values, indicating unique mechanical properties. Stable materials tend to have higher values of both moduli, indicating good mechanical resilience. The correlation between bulk and shear moduli suggests that materials with high resistance to compression also resist shape changes well. Figure 5 shows the combined stability of the materials.

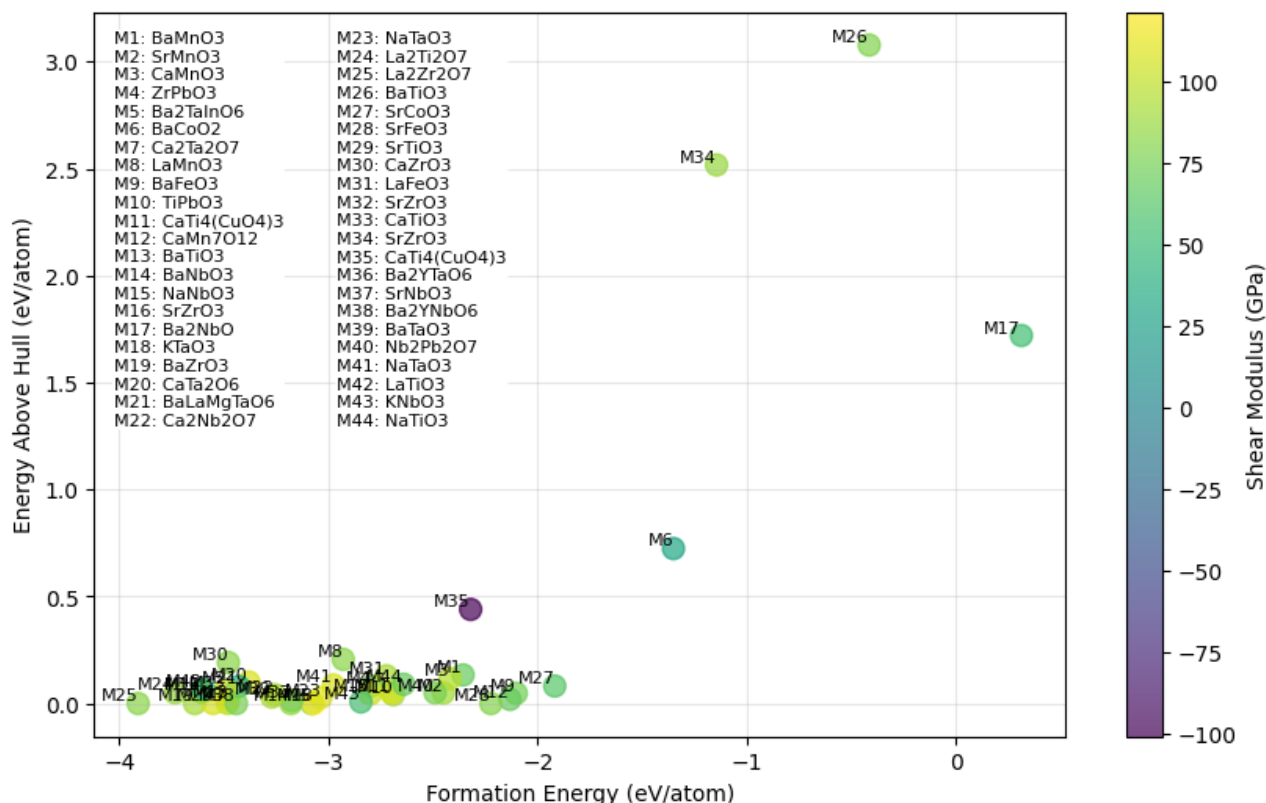


Figure 5. Combined thermodynamic and mechanical stability of materials

Most materials are clustered near the origin, indicating both high thermodynamic stability and ductility. A few outliers show distinct properties, for example, BaTiO₃ (M26) having high ductility and Ba₂NbO (M17) being less stable thermodynamically. Stable and ductile materials are near the origin with low E_{hull} and high Pugh’s ratio. Stable and brittle materials have low E_{hull} but lower Pugh’s ratio. This index is useful for identifying materials that balance both thermodynamic and mechanical stability, which is crucial for applications requiring durability and resilience. Figure 6 shows the radar plot for KTaO₃ (M18), which provides a visual representation of its key properties.

Bulk Modulus VRH (GPa) indicates the material’s resistance to uniform compression. The plot shows a moderate to high value, suggesting good mechanical stability. Shear Modulus VRH (GPa) reflects resistance to shape changes. The value is also moderate, supporting mechanical resilience. Energy Above Hull (eV/atom) represents thermodynamic stability. The plot shows a relatively low value, indicating good stability. Pugh’s Ratio indicates ductility. The plot shows a moderate value, suggesting a balance between ductility and brittleness. The plot is fairly balanced, with no extreme values, indicating that the material has a good balance of properties. The shaded area represents the overall performance across these parameters, with a larger area generally indicating better combined stability. Figure 7 shows the grid radar plot for material indices 14, 23, 35, and 39, as well as other candidates with good combined indices.

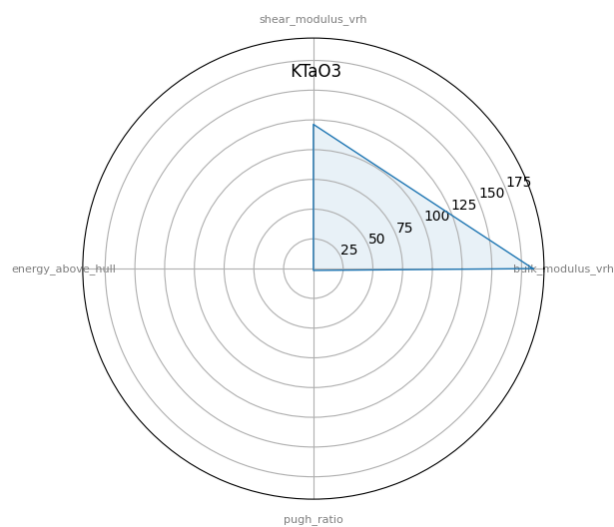


Figure 6. Radar plot of the combined index for KTaO₃

4. Discussion

Integrating thermodynamic and mechanical stability metrics into a unified framework has revealed critical insights into the design of perovskites for advanced applications. By analyzing 44 perovskites with complete datasets, this study demonstrates that materials such as KtaO₃, Ba₂TalnO₆, and BaNbO₃ exhibit balanced stability profiles, positioning them as promising candidates for applications requiring both durability and performance.

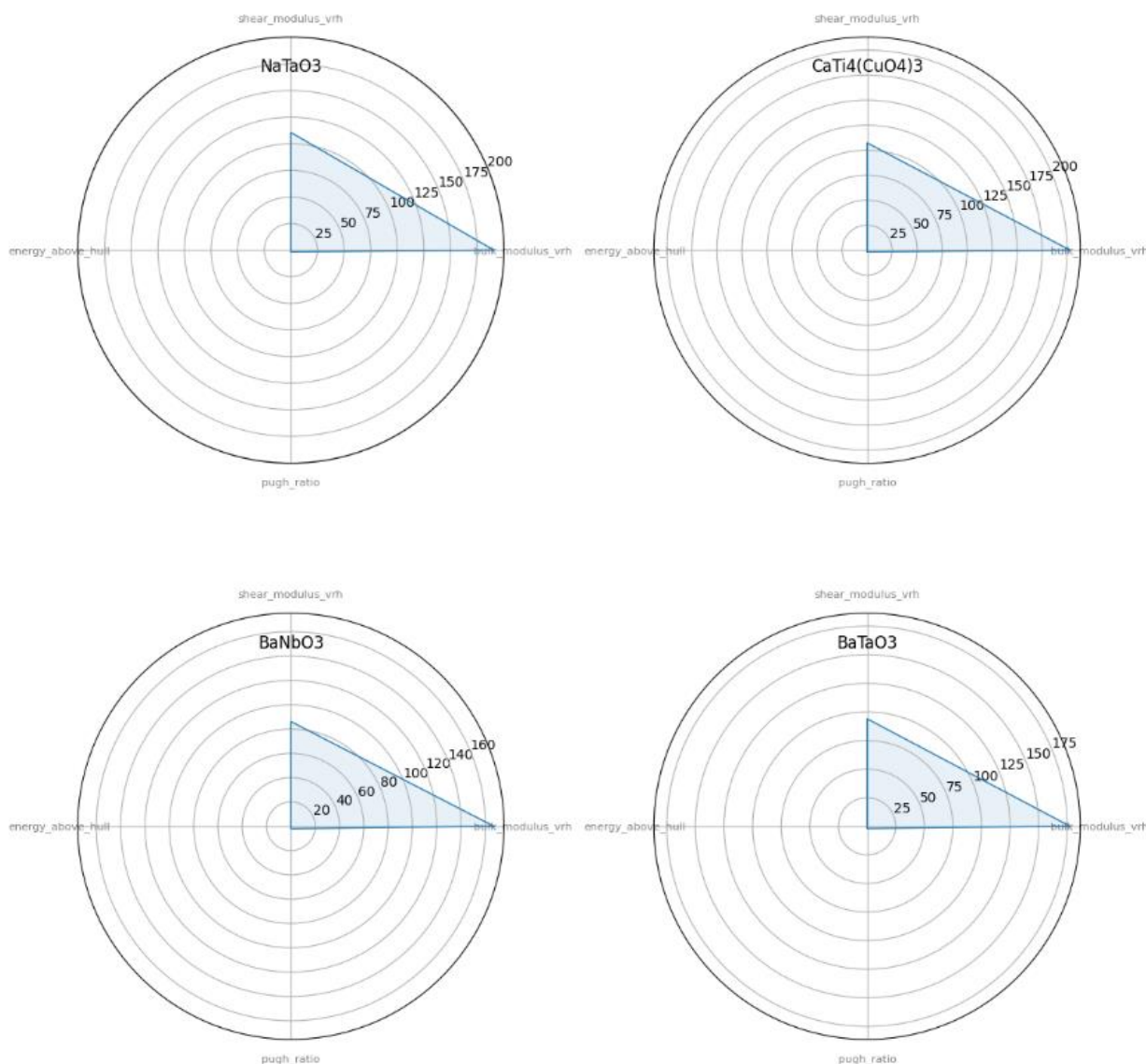


Figure 7. The grid radar plot for material index-14, 23, 35 and 39

The combined stability index successfully identifies materials that excel in both thermodynamic and mechanical stability. For instance, KTaO_3 (M18) achieves low energy above hull (0 eV/atom) and moderate mechanical properties (bulk modulus = 184.6 GPa, shear modulus = 121.3 GPa), reflecting its resistance to decomposition and mechanical stress. This balance is critical for applications like solar cells, where operational stresses (e.g., thermal cycling) demand materials that remain structurally intact over time. The dominance of Ba-based perovskites (e.g., BaTiO_3 , BaZrO_3) in the top candidates aligns with prior studies highlighting the stabilizing role of large A-site cations like Ba^{2+} , which reduce lattice distortions and enhance mechanical resilience [5,7]. Tantalum-containing perovskites (e.g., $\text{Ba}_2\text{TaNbO}_6$) consistently outperform their niobium counterparts (e.g., BaNbO_3) in combined stability metrics.

This is attributed to Ta^{5+} 's higher electronegativity and stronger metal-oxygen bonding, which enhances both thermodynamic stability (lower E_{hull}) and mechanical properties (higher bulk/shear moduli) [26]. These findings underscore the importance of B-site cation selection in tailoring stability. The Pugh's ratio distribution (Figure 2) reveals that most materials (~70%) are ductile ($B/G > 1.75$), a desirable trait for flexible electronics. However, brittle materials like $\text{Ca}_2\text{Ta}_2\text{O}_7$ (M7) still rank highly due to exceptional thermodynamic stability ($E_{\text{hull}} = 0.0008$ eV/atom), illustrating that application-specific requirements should guide material selection. For instance, brittle but thermodynamically stable perovskites may suffice for rigid photovoltaic panels, while ductile materials are preferable for wearable devices. The geometric mean-based combined index penalizes extreme weaknesses in any stability dimension, favoring balanced performance.

For example, SrFeO₃ (M28) achieves the highest combined index (99.5) due to its moderate E_{hull} (0 eV/atom) and exceptional mechanical properties ($B=128.6$ GPa, $G=80.35$ GPa). However, outliers like BaTiO₃ (M13) with higher E_{hull} (0.0148 eV/atom) but superior ductility ($B/G=1.62$) highlights the need for customizable weighting schemes in the index to prioritize specific properties for targeted applications.

5. Limitations and future work

This study offers valuable insights into the stability of perovskite materials, yet several limitations must be acknowledged: The analysis does not account for the influence of temperature and pressure on material stability, which can be significant in real-world applications, the impact of defects, which can greatly affect stability, is not included in this study, the dataset is limited to a few materials, restricting the exploration of other potentially stable structures. Expanding the dataset to thousands of perovskites using high-throughput DFT could uncover novel candidates with rare stability profiles, such as materials combining ultralow E_{hull} and extreme ductility. While DFT-derived metrics provide valuable insights, experimental validation of mechanical properties (e.g., nanoindentation for hardness) and thermodynamic stability (e.g., calorimetry) is essential to confirm computational predictions. Training machine learning models on stability metrics could accelerate the discovery of composition-structure-property relationships, particularly for non-cubic perovskites [12]. Customizing the combined index weights (e.g., prioritizing mechanical stability for aerospace materials or thermodynamic stability for high-temperature catalysts) would enhance its practical utility.

6. Conclusions

This comprehensive investigation into perovskite materials has provided valuable insights into the interplay between composition, structure, thermodynamic stability, and mechanical properties. Through systematic computational analysis of 44 distinct perovskite compositions, several promising candidates for technological applications were identified. The analysis highlights the superior stability profiles of tantalum-containing materials, suggesting that 5d transition metals may enhance both thermodynamic and mechanical stability due to stronger and more directional bonding characteristics. This trend underscores the potential advantages of incorporating such elements into perovskite structures. The observed relationships between formation energy and mechanical properties, such as bulk modulus, suggest fundamental structure-property correlations that can guide future material design. Materials with more negative formation energies tend to exhibit higher elastic moduli, indicating that stronger bonding contributes to both thermodynamic and mechanical stability. This work lays the groundwork for targeted experimental validation of the identified promising compositions. Future efforts should focus on synthesizing and characterizing these top candidates, particularly those containing tantalum, to verify the predicted properties and assess their performance under application-relevant conditions. Additionally, extending this computational framework to include dopants and defects could further enhance the stability and functional properties of these promising perovskite materials. By this work, the combined stability assessment approach has successfully identified materials that balance thermodynamic and mechanical

stability, providing a rational basis for the development of next-generation perovskite materials for diverse technological applications.

Ethical issue

The author is aware of and complies with best practices in publication ethics, specifically with regard to authorship (avoidance of guest authorship), dual submission, manipulation of figures, competing interests, and compliance with policies on research ethics. The author adheres to publication requirements that the submitted work is original and has not been published elsewhere.

Data availability statement

The manuscript contains all the data. However, more data will be available upon request from the author.

Conflict of interest

The author declares no potential conflict of interest.

References

- [1] L. Sanga, C. Lalengmawia, Z. Renthlei, S. T. Chanu, L. Hima, N. S. Singh, A. Yvaz, S. Bhattarai, D.P. Rai, (2025). A review on perovskite materials for photovoltaic applications, *Next Materials*, 7, 100494. doi.org/10.1016/j.nxmate.2025.100494.
- [2] Q. Sun and W.-J. Yin, (2017). Thermodynamic Stability Trend of Cubic Perovskites, *J. of the American Chem. Society*, 139:42, 14905-14908. doi.org/10.1021/jacs.7b09379.
- [3] W. Li, R. Jacobs, D. Morgan, (2018). Predicting the thermodynamic stability of perovskite oxides using machine learning models, *Computational Materials Science*, 150, 454-463, doi.org/10.1016/j.commatsci.2018.04.033.
- [4] S. Kim, T. Eom, Y.-S. Ha, K.-H. Hong, and H. Kim, (2020). Thermodynamics of Multicomponent Perovskites: A Guide to Highly Efficient and Stable Solar Cell Materials, *Chemistry of Materials*, 32:10, 4265-4272, doi.org/10.1021/acs.chemmater.0c00893.
- [5] Z. U. Rehman and Z. Lin, (2024). First-principles investigation of the structural stability, electronic, and thermodynamic properties of Ba₂NaHaO₆ (Ha = Cl, Br, I) periodate double perovskites, *J. Mater. Chem. A*, 12, 8846-8861, doi.org/10.1039/D3TA06721A.
- [6] S. Belhachi, S. Al-Qaisi, S. Samah, H. Rached, A. Zaman, T. A. Alrebdi, A. Boutramane, N. Erum, R. Ahmed & A. S. Verma, (2025). DFT Analysis of Ba₂NbRhO₆: A Promising Double Perovskite for Sustainable Energy Applications, *J Inorg Organomet Polym*, 35, 978-993, doi.org/10.1007/s10904-024-03336-5.
- [7] Md. F. Rahman, Md. H. Rahman, A. Kuddus, A. R. Chaudhry, and A. Irfan, (2024). Unveiling the Structural, Electronic, Optical, Mechanical, and Photovoltaic Properties of Lead-Free Inorganic New Ba₃MBr₃ (M = As, N, P, and Sb) Perovskites, *Energy & Fuels*, 38:8, 7260-7278, doi.org/10.1021/acs.energyfuels.4c00084.
- [8] S. Körbel, M. A. L. Marques and S. Botti, (2016). Stability and electronic properties of new inorganic perovskites from high-throughput ab initio calculations, *J. Mater. Chem. C*, 4, 3157-3167, doi.org/10.1039/C5TC04172D.

- [9] D. Pottmaier, E. R. Pinatel, J. G. Vitillo, S. Garroni, M. Orlova, M. D. Baró, G. B. M. Vaughan, M. Fichtner, W. Lohstroh, and M. Baricco, (2011). Structure and Thermodynamic Properties of the NaMgH₃ Perovskite: A Comprehensive Study, *Chemistry of Materials*, 23:9, 2317-2326, doi.org/10.1021/cm103204p.
- [10] R. Lu, A. M. Hofmeister, Y. Wang, (1994). Thermodynamic properties of ferromagnesium silicate perovskites from vibrational spectroscopy, *Journal of Geophysical Research: Solid Earth*, 99:B6, 11795-11804, doi.org/10.1029/94JB00501.
- [11] B. A. Rosales, K. Schutt, J. J. Berry, and L. M. Wheeler, (2023). *ACS Energy Letters*, 8:4, 1705-1715, doi.org/10.1021/acscenergylett.2c02698.
- [12] R. Jaafreh, A. Sharan, M. Sajjad, N. Singh, K. Hamad, (2023). A Machine Learning-Assisted Approach to a Rapid and Reliable Screening for Mechanically Stable Perovskite-Based Materials, *Adv. Funct. Mater.*, 33, 2210374, doi.org/10.1002/adfm.202210374.
- [13] F. Song, D. Zheng, J. Feng, J. Liu, T. Ye, Z. Li, K. Wang, S. F. Liu, D. Yang, (2024). Mechanical Durability and Flexibility in Perovskite Photovoltaics: Advancements and Applications, *Adv. Mater.*, 36, 2312041, doi.org/10.1002/adma.202312041.
- [14] N. Rolston, A. D. Printz, J. M. Tracy, H. C. Weerasinghe, D. Vak, L. J. Haur, A. Priyadarshi, N. Mathews, D. J. Slotcavage, M. D. McGehee, R. E. Kalan, K. Zielinski, R. L. Grimm, H. Tsai, W. Nie, A. D. Mohite, S. Gholipour, M. Saliba, M. Grätzel, R. H. Dauskardt, (2018). Effect of Cation Composition on the Mechanical Stability of Perovskite Solar Cells, *Adv. Energy Mater.*, 8, 1702116, doi.org/10.1002/aenm.201702116.
- [15] A.S. Verma, A. Kumar, (2012). Bulk modulus of cubic perovskites, *J. of Alloys and Compounds*, 541, 210-214, doi.org/10.1016/j.jallcom.2012.07.027.
- [16] J. Kung & S. Rigden, (1999). Oxide perovskites: pressure derivatives of the bulk and shear moduli, *Phys Chem Min*, 26, 234-241, doi.org/10.1007/s002690050182.
- [17] J. Yu, M. Wang, and S. Lin, (2016). Probing the Soft and Nanoductile Mechanical Nature of Single and Polycrystalline Organic-Inorganic Hybrid Perovskites for Flexible Functional Devices, *ACS Nano*, 10:12, 11044-11057, doi.org/10.1021/acsnano.6b05913.
- [18] Y. Gupta, S. Rathore, A. Singh, A. Kumar, (2022). Tailoring the mechanical response of Ruddlesden Popper lead halide perovskites, *J. of Alloys and Compounds*, 901, 163575, doi.org/10.1016/j.jallcom.2021.163575.
- [19] A. Bakar, A. O. Alrashdi, M. M. Fadhali, A. Afaq, H.A. Yakout, M. Asif, (2022). Effect of pressure on structural, elastic and mechanical properties of cubic perovskites XCoO₃ (X = Nd, Pr) from first-principles investigations, *J. of Materials Research and Technology*, 19, 4233-4241, doi.org/10.1016/j.jmrt.2022.06.126.
- [20] M. Boubchir, R. Boubchir, H. Aourag, (2022). The Principal Component Analysis as a tool for predicting the mechanical properties of Perovskites and Inverse Perovskites, *Chemical Physics Letters*, 798, 139615, doi.org/10.1016/j.cplett.2022.139615.
- [21] J.Y. Al-Humaidi, Abdullah, Amina, J. Akhtar, A. Algahtani, V. Tirth, S. Abdullaev, M. S. Refat, M. Aslam & A. Zaman, (2024). Electronic Structural, Optical and Elastic Properties of K-Based Lead-Free Perovskites KXF₃ (X = Nb, Ti, Zr) via DFT Computational Approach, *J Inorg Organomet Polym*, 34, 1643-1653, doi.org/10.1007/s10904-023-02905-4.
- [22] P. Sánchez-Palencia, G. García, P. Wahnón and P. Palacios, (2021). The effects of the chemical composition on the structural, thermodynamic, and mechanical properties of all-inorganic halide perovskites, *Inorg. Chem. Front.*, 8, 3803-3814, doi.org/10.1039/D1QI00347J.
- [23] S. A. Khandy, I. Islam, D. C Gupta, R. Khenata, A. Laref and S. Rubab, (2018). DFT understandings of structural properties, mechanical stability and thermodynamic properties of BaCfO₃ perovskite, *Mater. Res. Express*, 5, 105702, doi.org/10.1088/2053-1591/aad9eb.
- [24] E. K. Mahmoud, A. A. Farghali, S. I. El-dek & M. Taha, (2022). Structural stabilities, mechanical and thermodynamic properties of chalcogenide perovskite ABS₃ (A = Li, Na, K, Rb, Cs; B = Si, Ge, Sn) from first-principles study, *Eur. Phys. J. Plus*, 137, 1006 doi.org/10.1140/epjp/s13360-022-03211-7.
- [25] T. I. Al-Muhimeed, (2024). Study of mechanical, thermodynamic, thermoelectric, and optical properties of Cs₂SbAuX₆ (X = Cl, Br, I) for energy harvesting applications, *Materials Processing*, 78, 108443, doi.org/10.1016/j.mssp.2024.108443.
- [26] Q. Dai, Q.-Q. Liang, T.-Y. Tang, H.-X. Gao, S.-Q. Wu, Y.-L. Tang, (2024). The structural, stability, electronic, optical and thermodynamic properties of Ba₂AsXO₆ (X = V, Nb, Ta) double perovskite oxides: A First-Principles study, *Inorganic Chemistry Communications*, 166, 112591, doi.org/10.1016/j.inoche.2024.112591.
- [27] S. A. Khandy, D. C. Gupta, (2020). Magneto-electronic, mechanical, thermoelectric and thermodynamic properties of ductile perovskite Ba₂SmNbO₆, *Materials Chemistry and Physics*, 239, 121983, doi.org/10.1016/j.matchemphys.2019.121983.
- [28] P. Zhang, B. Chen, W. Zhu, C. Wang, W. Zhang, Y. Li & W. Liu, (2020). First-principles prediction of structural, mechanical and thermal properties of perovskite BaZrS₃, *Eur. Phys. J. B*, 93, 97 doi.org/10.1140/epjb/e2020-10082-9.
- [29] The Materials Project, (2025). <https://next-gen.materialsproject.org/materials>, Accessed on 03.12.2025.
- [30] AFLOW, (2025). Aflow - Automatic FLOW for Materials Discovery, <https://afwlib.org/>, accessed on 03.15.2025.
- [31] A. Lamichhane, (2021). First-principles density functional theory studies on perovskite materials. PhD thesis. New Jersey Institute of Technology, 2021. 28321795. Retrieved from <https://www.proquest.com/dissertations->

- theses/first-principles-density-functional-theory/docview/2556353068/se-2.
- [32] Q. Wei, H. Liang, Y. Haruta, M. Saidaminov, Q. Mi, M. Saliba, G. Cui, Z. Ning, (2023). From tetragonal to cubic: perovskite phase structure evolution for high-performance solar cells, *Science Bulletin*, 68:2, 141-145, doi.org/10.1016/j.scib.2023.01.008.
- [33] G. King and P. M. Woodward, (2010). Cation ordering in perovskites, *J. Mater. Chem.*, 20, 5785-5796, doi.org/10.1039/B926757C.
- [34] M. P. Hautzinger, W. Mihalyi-Koch, and S. Jin, (2024). A-Site Cation Chemistry in Halide Perovskites, *Chem. of Materials*, 36:21, 10408-10420, doi.org/10.1021/acs.chemmater.4c02043
- [35] G. E. Eperon and D. S. Ginger, (2017). B-Site Metal Cation Exchange in Halide Perovskites, *ACS Energy Letters*, 2:5, 1190-1196, doi.org/10.1021/acseenergylett.7b00290.
- [36] D. J. Singh, M. Ghita, M. Fornari, & S. V. Halilov, (2006). Role of A-Site and B-Site Ions in Perovskite Ferroelectricity. *Ferroelectrics*, 338:1, 73-79. doi.org/10.1080/00150190600732694.
- [37] VASP, (2025). The Vienna Ab initio Simulation Package: atomic scale materials modelling from first principles, <https://www.vasp.at/>, accessed on 03.12.2025.
- [38] M. Ernzerhof, G. E. Scuseria; (1999) Assessment of the Perdew–Burke–Ernzerhof exchange–correlation functional, *J. Chem. Phys.*, 110:11, 5029–5036. doi.org/10.1063/1.478401.
- [39] A. A. Awan, (2022). 21 Essential Python Tools, <https://www.datacamp.com/tutorial/21-essential-python-tools>, accessed on 12.03.2025.
- [40] A.-R. A. Ragab, S. E. A. Bayoumi, (1998). *Engineering Solid Mechanics: Fundamentals and Applications*, CRC Press, ISBN 10: 0849316073.
- [41] H. Li, Y. Chen, H. Wang, H. Wang, Y. Li, I. Harran, Y. Li, C. Guo, (2017). First-principles study of mechanical and thermodynamic properties of Ti-Ga intermetallic compounds, *J. of Alloys and Compounds*, 700, 208-214, doi.org/10.1016/j.jallcom.2017.01.052.
- [42] X.-Q. Chen, H. Niu, D. Li, Y. Li, (2011). Modeling hardness of polycrystalline materials and bulk metallic glasses, *Intermetallics*, 19:9, 1275-1281, doi.org/10.1016/j.intermet.2011.03.026.
- [43] S. I. Ranganathan and M. Ostoja-Starzewski, (2008). Universal Elastic Anisotropy Index, *Phys. Rev. Lett.*, 101, 055504, doi.org/10.1103/PhysRevLett.101.055504.
- [44] I. H. Siegel, (1942). Index-Number Differences: Geometric Means. *J. of the American Statistical Association*, 37:218, 271–274, doi.org/10.1080/01621459.1942.10500636.



This article is an open-access article distributed under the terms and conditions of the Creative Commons Attribution (CC BY) license (<https://creativecommons.org/licenses/by/4.0/>).